ACS APPLIED MATERIALS & INTERFACES

Research Article

Cite This: ACS Appl. Mater. Interfaces 2017, 9, 44060−44069

www.acsami.org

# Effect on Electrode Work Function by Changing Molecular Geometry of Conjugated Polymer Electrolytes and Application for Hole-Transporting Layer of Organic Optoelectronic Devices

Eui Jin Lee,[‡] Min Hee Choi,[§] Yong Woon Han,[†] and Doo Kyung Moon*[,†]

[†]Department of Materials Chemistry and Engineering, Konkuk University, 120, Neungdong-ro, Gwangjin-gu, Seoul 05029, Republic of Korea

[‡]Convergence Research Center for Solar Energy, Daegu Gyeongbuk Institute of Science and Technology, 333, Techno Jungang daero, Dalseong-gun, Daegu 42988, Republic of Korea

[§]Progressive Technology Research Group, KOLON Central Research Park, 30, Mabuk-ro 154beon-gil, Giheung-gu, Yongin-si 16910, Gyeonggi-do, Republic of Korea

Supporting Information

**ABSTRACT:** In this study, we synthesized three conjugated polymer electrolytes (CPEs) with different conjugation lengths to control their dipole moments by varying spacers. P-type CPEs (PFT-D, PFtT-D, and PFbT-D) were generated by the facile oxidation of n-type CPEs (PFT, PFtT, and PFbT) and introduced as the hole-transporting layers (HTLs) of organic solar cells (OSCs) and polymer light-emitting diodes (PLEDs). To identify the effect on electrode work function tunability by changing the molecular conformation and arrangement, we simulated density functional theory calculations of these molecules and performed ultraviolet photoelectron spectroscopy analysis for films of indium tin oxide/CPEs. Additionally, we fabricated OSCs and PLEDs using the CPEs as the HTLs. The stability and performance were enhanced in the optimized devices with PFtT-D CPE HTLs compared to those of PEDOT:PSS HTL-based devices.

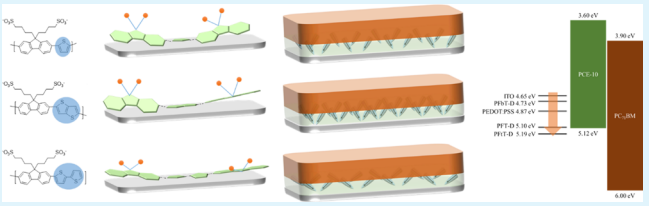

**KEYWORDS:** *organic optoelectronic devices, stability, hole-transporting layer, conjugated polymer electrolytes, molecular dipole*

## INTRODUCTION

Organic optoelectronic devices (OOEDs), which can convert light into electricity (organic solar cells, OSCs) or electricity into light (organic light-emitting diodes, OLEDs), have attracted tremendous academic and industrial attention for sustainable energy conversion applications.[1−4] Recently, with the research and development of various organic semiconducting materials and device structures, the efficiency and stability of OOEDs have improved dramatically.[5−11] The power conversion efficiency (PCE) of OSCs is more than 11%, a level acceptable for commercialization.[5,9,12] Prototypes and commercial applications of OLEDs in lighting and displays have already been developed.

The device structures, including the materials and the functions of each layer in OSCs and OLEDs, which typically consist of substrates, transparent electrodes, buffer layers, and organic active layers, are almost same. Because of this structural, material, and functional similarity, studies on OSCs and OLEDs are complementary in nature. For example, conjugated polymer electrolytes (CPEs)[13,14] and transition-metal oxides[15] have been investigated as buffer materials in OOEDs to facilitate the transportation of charge carriers (electrons or holes).

In terms of the efficiency and stability of OOEDs, charge transport, which means the extraction of charge carriers for OSCs and the injection of carriers for OLEDs, is a critical factor. Therefore, controlling the interfacial properties of each layer is necessary to obtain highly efficient and stable devices. By understanding and improving charge transport via interfacial engineering, the performance and long-term stability of OOEDs have progressed.[13,14,16−18]

To promote the transportation of charge carriers and enhance the performance of OOEDs, electron- or hole-transport layers are introduced above or below the organic active layers. Zirconium acetylacetonate (ZrAcac),[19] cesium carbonate ($Cs_2CO_3$),[20] and conjugated organic compounds, for example, poly[(9,9-bis(3′-(*N*,*N*-dimethylamino)propyl)-2,7-fluorene)-*alt*-2,7-(9,9-dioctylfluorene)] (PFN),[21] 3,3′,3″,3‴-((pyrene-1,3,6,8-tetrayltetrakis(benzene-4,1-diyl))tetrakis(oxy))tetrakis(*N*,*N*-dimethylpropan-1-amine),[22] and 3,6-bis(5-(4-(3-(dimethylamino)propoxy)-phenyl)thiophen-2-yl)-2,5-bis(2-hexyl-decyl)pyrrolo[3,4-*c*]pyrrole-1,4(2*H*,5*H*)-dione,[23] have been introduced as electron-transport layer (ETL) of OOEDs. Specifically, PFN and derivatives thereof are commonly sold by suppliers like 1-materials, Lumtec, and Ossila.

However, materials for hole-transport layers (HTLs), which should be soluble in both water and alcohols to avoid

Received: July 28, 2017
Accepted: November 21, 2017
Published: November 21, 2017






DOI: 10.1021/acsami.7b11164
ACS Appl. Mater. Interfaces 2017, 9, 44060−44069

**Scheme 1. Polymerization Process of CPEs**

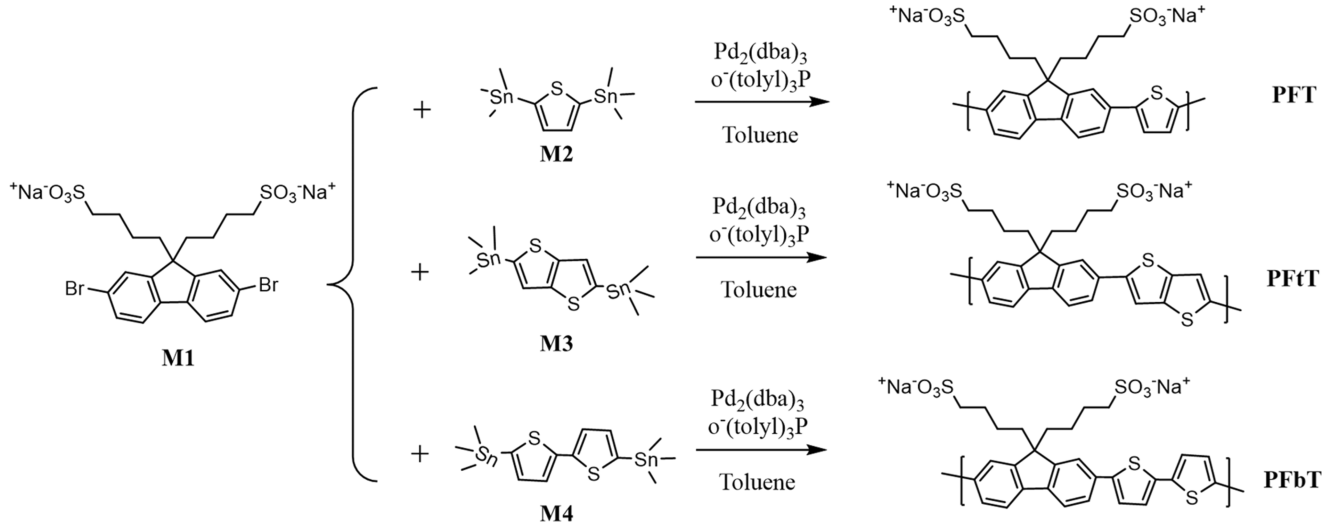


intermixing with the organic active layers for multilayer-structure devices, are very limited. Poly(3,4-ethylenedioxythiophene):polystyrene sulfonate (PEDOT:PSS) is an extensively used material for HTL and transparent electrode because of its remarkable electrical conductivity, optical properties, and solution processability.[24−28] However, PEDOT:PSS accelerates the degradation of devices because it is both acidic and hygroscopic.[24] To replace PEDOT:PSS, studies on transition-metal oxide precursors for molybdenum oxide ($MoO_x$),[29] nickel oxide ($NiO_x$),[30] tungsten oxide ($WO_3$),[31] and organic materials, such as conjugated polymer electrolytes[32−36] and small molecules,[37,38] have been performed. The results of these reported works exhibit comparable performance to PEDOT:PSS-based devices. However, transition-metal oxides for solution processing have some disadvantages, including high annealing temperatures, surface defects, and hydrophilicity.[29−31,39] CPEs, which consist of conjugated polymeric main chain and branched ionic pendant groups, can form molecular dipole moments at the interface of organic active layer/anode or cathode for charge transport and energy-level control. Moreover, CPEs can be dissolved in alcohols and neutral-pH water, and high-temperature thermal annealing is unnecessary during HTL formation. For this reason, they are regarded as suitable materials for printing processes to fabricate flexible OOEDs as replacements for PEDOT:PSS HTLs.

In this study, we synthesized three CPEs of poly[9,9-bis(4′-sulfonatobutyl)fluorene-*alt*-thiophene] (PFT), poly[9,9-bis(4′-sulfonatobutyl)fluorene-*alt*-thieno[3,2-*b*]thiophene] (PFtT), and poly[9,9-bis(4′-sulfonatobutyl)fluorene-*alt*-2,2′bithiophene] (PFbT) with different conjugation lengths to control their dipole moments by varying spacers. The n-type CPEs were oxidized by $Na_2S_2O_8$ oxidant to form p-type CPEs (PFT-D, PFtT-D, and PFbT-D) containing radical cations (i.e., polarons) in their main chain.[40] The self-doped p-type CPEs, comprising $\pi$-conjugated polymeric chains with ionic pendant groups, can reduce the energy barrier, which can be generated by different energy levels between anode and organic semiconducting materials in organic electronic devices. To achieve high performance, matching energy levels at interfaces is essential. To identify the effect on the dipole moment and electrode work function tunability by changing the molecular conformation and arrangement, we performed density functional theory (DFT) calculations of these molecules and ultraviolet photoelectron spectroscopy (UPS) analysis of indium tin oxide (ITO)/CPE films. Additionally, we fabricated OSCs and polymer light-emitting diodes (PLEDs), by introducing the CPEs as the HTLs. In comparison to the reference device in which the PEDOT:PSS was used as HTL, the stability and performance of the device with the PFtT-D CPE HTL were enhanced.

## EXPERIMENTAL SECTION

**Synthesis of CPEs.** *Synthesis of Monomers.* The materials purchased from Sigma-Aldrich and Alfa Aesar were employed for all reaction and polymerization processes, without further purification. The reported methods[40] were modified to synthesize sodium 4-(2,7-dibromo-9-(4-sulfonatobutyl)-9*H*-fluoren-9-yl)butyl sulfite (M1).

*Polymerization.* Dimethylformamide (DMF, 54 mL) was used as solvent to dissolve monomer M1 (2.0 mmol) and M2 (or M3 or M4) (2.0 mmol). The vessel containing the result solution was purged with nitrogen for 15 min to eliminate oxygen and moisture. Then, tris(dibenzylideneacetone)dipalladium(0) ($Pd_2dba_3$) (0.1 mmol, 5 mol %) and tri-(*o*-tolyl)phosphine (0.4 mmol, 20 mol %) were mixed with the above solution. The temperature of the mixture was elevated to 100 °C and kept for 48 h before being poured into 300 mL of acetone. The yellow products were collected by vacuum filtration and rinsed with acetone (300 mL, twice). The collected products were then dissolved in water to be purified through cellulose membranes (12 kD molecular-weight cutoff). After purification, the solvent was eliminated by the low-temperature drying method (Scheme 1).

*Poly[9,9-bis(4′-sulfonatobutyl)fluorene-alt-thiophene] (PFT).* Yellow solid, 0.65 g (yield = 58%). $^1$H NMR (400 MHz, DMSO-*d*, d): $\delta$ 7.85 (d, 2H), 7.68 (s, 2H), 2.35 (m, 2H), 2.14 (s, 3H), 2.08 (s, 2H), 1.56 (m, 2H), 1.42 (m, 4H), 0.56 (m, 2H). GPC in buffer pH 9 + 30% MeOH: MW 10 980 Da

*Poly[9,9-bis(4′-sulfonatobutyl)fluorene-alt-thieno[3,2-b]-thiophene] (PFtT).* Yellow solid, 0.50 g (yield = 40%). $^1$H NMR (400 MHz, DMSO-*d*, d): $\delta$ 7.84 (d, 2H), 7.65 (d, 2H), ∼7.43−7.31 (m, 2H), 2.33 (s, 2H), 2.12 (d, 2H), 2.08 (s, 2H), 1.56 (m, 2H), 1.38 (s, 4H), 0.64−0.52 (m, 2H). GPC in buffer pH 9 + 30% MeOH: MW 20 961 Da

*Poly[9,9-bis(4′-sulfonatobutyl)fluorene-alt-2,2′bithiophene] (PFbT).* Yellow solid, 0.62 g (yield = 48%). $^1$H NMR (400 MHz, DMSO-*d*, d): $\delta$ 8.02 (d, 2H), 7.87 (m, 2H), 7.66 (d, 2H), ∼7.48−7.26 (m, 1H), 2.41−2.32 (m, 2H), 2.14 (m, 2H), 2.08 (s, 2H), 1.52 (m, 2H), 1.42 (m, 4H), 0.65−0.50 (m, 4H). GPC in buffer pH 9 + 30% MeOH: MW 16 925 Da


DOI: 10.1021/acsami.7b11164
ACS Appl. Mater. Interfaces 2017, 9, 44060−44069

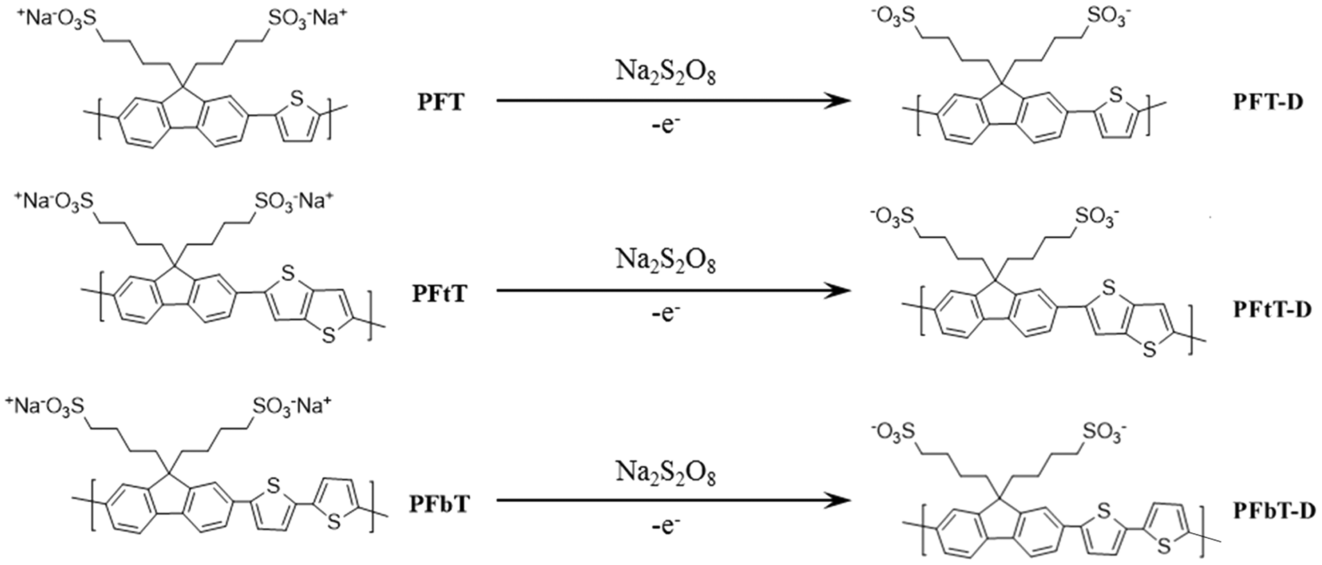


**Figure 1.** Preparation process of CPEs.

*Preparation of PFT-D, PFtT-D, and PFbT-D.* $Na_2S_2O_8$ (3 mol) was dissolved in 1 mL of $H_2O$, and 1 mL of 5 mg/mL aqueous solution of PFT, PFtT, or PFbT was then added to the first solution. The solutions were mixed and reacted at room temperature for over 2 h. The result solutions were filtered by vacuum filtration. The collected powders were rinsed with acetone and cold $H_2O$ several times. The products were dried in a vacuum oven, and pale yellow solids were obtained.

*Fabrication of OSCs.* Before fabrication process of the OSC devices, patterned ITO glass substrates were cleaned and surface-treated through a previously reported method.[39,41] For the HTL solution, PFT-D, PFtT-D, and PFbT-D were each dissolved at various concentrations in absolute methanol (HPLC grade) and filtered through a 0.45 $\mu$m poly(tetrafluoroethylene) (PTFE) syringe filter. The filtered solutions and PEDOT:PSS (Heraeus, P VP AI 4083) were spin-coated at 3000 rpm for 30 s onto individual ITO surfaces as HTL. The thickness of CPE HTLs was calculated by a previously reported method (see Figure S1 of Supporting Information).[42,43] The optimal annealing temperatures for CPEs and PEDOT:PSS HTL were 70 and 140 °C, respectively. The solution in which poly[4,8-bis(5-(2-ethylhexyl)thiophen-2-yl)benzo[1,2-*b*;4,5-*b*′]dithiophene-2,6-diyl-*alt*-(4-(2-ethylhexyl)-3-fluorothieno[3,4-*b*]thiophene)-2-carboxylate-2-6-diyl] (PCE-10, 1-materials) and [6,6]-phenyl $C_{71}$ butyric acid methyl ester ($PC_{71}BM$, 1-materials) (1:1.5, w/w) were dissolved in a mixed solvent of chlorobenzene and 1,8-diiodooctane additive (97:3 v/v) was employed on the HTLs by spin-coating in a $N_2$-filled glovebox, to form photoactive layers with thicknesses of 80 nm. To deposit electron extraction layers, PFN solution (2 mg/mL in methanol with 2 $\mu$L/mL of acetic acid) was used for spin-coating onto the photoactive layers. Finally, Al cathodes (100 nm) were thermally deposited under $<10^{-7}$ Torr high vacuum. The activated area (7 $mm^2$) of the OSCs was determined by sus mask.

*Fabrication of PLEDs.* To fabricate the PLEDs, we used green-yellow emitting polymers (Covion super-yellow). The PLEDs were fabricated with the same process as the OSCs, without the formation of emitting layers. In a $N_2$-filled glovebox, the solution of super-yellow at the concentration of 0.5 wt % in chlorobenzene was employed on each HTL by spin coating. The process of thermal annealing was performed at 120 °C on a hot plate for 30 min for the organic emitting layer with thickness of 80 nm. Finally, bilayer cathodes of Ba/Al (2/100 nm) were thermally deposited under $<10^{-7}$ Torr high vacuum. The determined emitting area of the PLEDs was 4 $mm^2$.

*Measurements.* An Alpha-Step 500 surface profiler (KLA-Tencor) and atomic force microscopy (AFM, PSIA XE-100, contact mode) were used for measuring the thicknesses of prepared thin films. The optical transmittances of the HTLs and the light absorption of PCE-10 were characterized using an ultraviolet−visible (UV−vis) spectrometer (Agilent 8453). The molecular conformations and arrangements of the CPEs on the substrates were assumed by DFT calculations, using Gaussian 09 with basis set of a hybrid B3LYP-correlation function and a split-valence 6-31G(d). The surface morphologies of the films were analyzed by AFM (PSIA XE-100, non-contact mode). The work function (WF) of the ITO/HTLs was measured by UV photoelectron spectroscopy (UPS, He I 21.2 eV). A source measurement unit (Keithley 2400) and an AM 1.5G solar simulator (Newport 96000 with 150 W xenon lamp) were used to identify the photovoltaic factors of the fabricated OSCs. The incident photon-to-current conversion efficiency (IPCE, McScience) was assessed for the optimal devices. The performance of the PLEDs was characterized using a Keithley 2400 and a PR 670 (Photo Research) spectral scanner.

## RESULTS AND DISCUSSION

Figure 1 exhibits the preparation of the CPEs. The structures of PFT-D, PFtT-D, and PFbT-D suggest that the ionic functional groups may be changed to $SO^{3-}$ by elimination of the $Na^+$ cations during oxidation. Although the degree of oxidization can be controlled by the concentration of the employed oxidants, not all of the repeating units are oxidized. The PFT, PFtT, and PFbT were oxidized with 3 M $Na_2S_2O_8$ in water for 2 h.[33] We show in Table S1 (see Supporting Information) the composition of these polymers, where the concentrations are given in weight percent (wt %), as characterized using the X-ray fluorescence technique. We limited our effort to the study of the two oxides of $Na_2O$ and $SO_3$ to confirm the $Na^+$ contents in the polymers. The oxidative doped polymers of PFT-D, PFtT-D, and PFbT-D showed lower $Na_2O$ and higher $SO_3$ rates than PFT, PFtT, and PFbT did. Figure S2 (Supporting Information) exhibits the optical absorption property of the PFT, PFtT, PFbT, PFT-D, PFtT-D, and PFbT-D solutions from UV−vis spectroscopy. The wavelengths at the maximum absorption peaks are listed in Table S2 (Supporting Information). The absorption bands of PFT, PFtT, and PFbT at 418, 430, and 454 nm correspond to the $\pi-\pi^*$ transitions from the valence band maximum to the conduction band minimum. It can be confirmed that excitation to the polaron state was progressed during the oxidation process, from the absorption edge at approximately 450−480 nm. This becomes more noticeable as the solvation effect of the employed oxidizing agent increases.


DOI: 10.1021/acsami.7b11164
ACS Appl. Mater. Interfaces 2017, 9, 44060−44069

The UV-absorption spectra of the n-type CPEs are blue-shifted after ion doping because conjugation with the polarons is broken.[44] PFT, PFtT, and PFbT show $\lambda_{max}$ at 355, 391, and 403 nm, respectively. For a polaron, because the localized electronic level location is dependent on the extent of the geometric change, bonding and antibonding are symmetrically formed at $\pm\omega_0$ for the gap center.[45] Therefore, we confirm that PFT-D, PFtT-D, and PFbT-D were oxidized successfully.

Figures 2 and S3 (see Supporting Information) exhibit the $J-V$ characteristics and IPCE data from the OSCs, respectively.

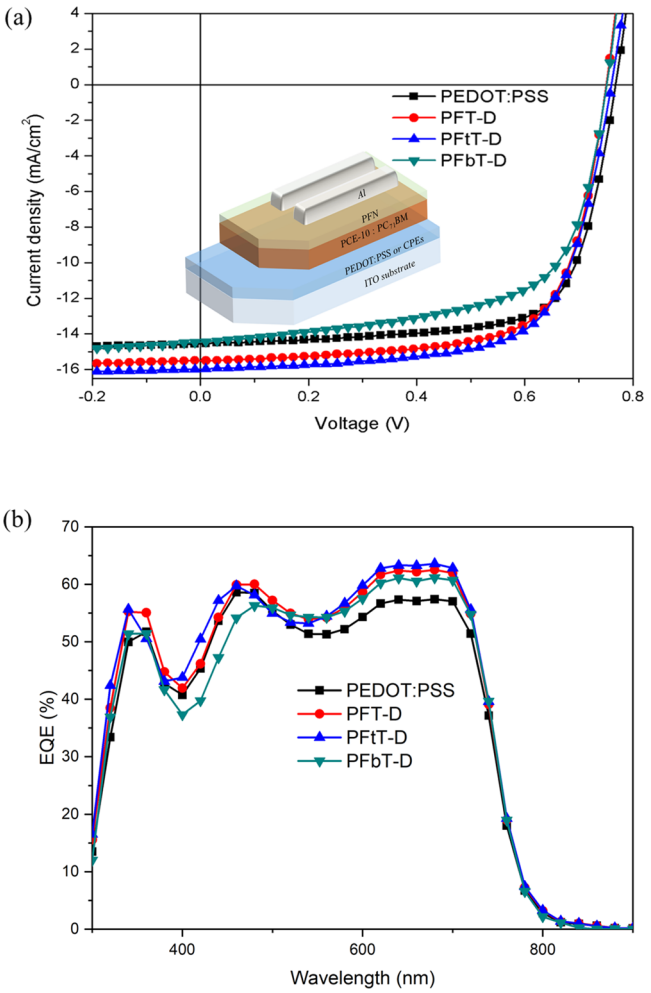


**Figure 2.** (a) $J-V$ characteristics and (b) IPCE data of OSCs.

The performances of the devices are listed in Tables 1, 2, and S3 (see Supporting Information). The reference device has the short-circuit current ($J_{sc}$) of 14.5 mA/cm$^2$, open-circuit voltage ($V_{oc}$) of 0.78 V, fill factor (FF) of 70.6%, and PCE of 8.0%.

**Table 1. Photovoltaic Performances of OSCs**[a]

| HTL | $J_{sc}$ (mA/cm$^2$) | $V_{oc}$ (V) | FF (%) | PCE (%) |
|---|---|---|---|---|
| PEDOT:PSS | 14.5 (14.4) | 0.78 (0.78) | 70.6 (69.4) | 8.0 (7.8) |
| PFT-D | 15.5 (15.5) | 0.76 (0.76) | 68.9 (67.5) | 8.1 (8.0) |
| PFtT-D | 16.0 (15.8) | 0.76 (0.76) | 68.4 (68.2) | 8.3 (8.2) |
| PFbT-D | 14.4 (14.1) | 0.76 (0.76) | 63.4 (62.0) | 6.9 (6.6) |

[a]The average values from four different devices are listed in parentheses.

**Table 2. Dihedral Angles of CPEs from DFT Calculation**

| CPEs | dihedral angle 1 (deg) | dihedral angle 2 (deg) | dihedral angle 3 (deg) |
|---|---|---|---|
| PFT-D | 152 | 151 | |
| PFtT-D | 152.4 | 152 | |
| PFbT-D | 154.9 | 161 | 155 |

The device with the PFtT-D CPE interlayer shows the best performance ($J_{sc}$ = 16.0 mA/cm$^2$, $V_{oc}$ = 0.76 V, FF = 68.4%, and PCE = 8.3%). The PFT-D also has performance comparable (8.1%) to that of the reference device. However, the performance of the device with the PFbT-D CPE decreases, with a considerable FF drop.

As shown in Figure 2b, the external quantum efficiency (EQE) of the devices with PFT-D and PFtT-D CPE HTLs were increased against the reference device. Interestingly, the EQE curves of the devices with CPEs exhibit different shape from the reference device. In the range of approximately 500–800 nm, the devices with CPEs showed increased EQE values compared to the reference device. It is because that light absorption and interference effect are different in CPEs and PEDOT:PSS at this range.

Figure S4a (see Supporting Information) shows the optical transmittance of the spin-coated HTLs on ITO electrode, and that of bare ITO is also contained to compare. The CPEs showed lower transmittance than PEDOT:PSS in the range of 378–507 nm. However, at longer wavelength than 507 nm, the CPEs on ITO showed higher transmittances than PEDOT:PSS on ITO. As exhibited in Figure S4b (Supporting Information), the donor polymer, PCE-10, mainly absorbs light at the wavelength range of 560–750 nm ($\lambda_{max}$ = 704 nm). Thus, increased light irradiation of the photoactive layer is expected. This absorption band contributes to the increased current density values of the PFT-D- and PFtT-D-based devices relative to those of the reference device, and the enhanced EQE of the device with PFbT-D relative to that of the reference device in the 500–800 nm range.

To understand the molecular conformation and arrangement of CPEs, the molecular geometries were simulated using DFT calculations. The calculations were performed using Gaussian 09. The results and schematics based on the calculated results are exhibited in Figure 3. The calculated dihedral angles between the fluorene and the thiophene or thienothiophene units were listed as shown in Table 2. In PFT-D and PFtT-D, the dihedral angles were similar, between 151 and 152.4°. However, PFbT-D had larger dihedral angles than the others. This means that PFbT-D has a more planar structure than the other CPEs. The conformation and orientation of molecules can affect the molecular dipole moment.[46,47] The anionic pendant groups of the CPEs can be rated as rigidly fixed dipoles attached to the polymeric backbones, forming molecular dipoles between the side-chain anionic functional groups and the backbones.[13,40,46] The dipole moments are strengthened for more aligned (planar) orientations.

To identify the effective WF changes at the surface of HTL-coated ITO electrodes, we performed UPS analysis. Figure S5 (see Supporting Information) shows the UPS spectra of each anode. The effective WF values ($\Phi$) of the electrodes were calculated using the following equation

$$\Phi = h\nu - E_{cutoff}$$



DOI: 10.1021/acsami.7b11164
ACS Appl. Mater. Interfaces 2017, 9, 44060–44069

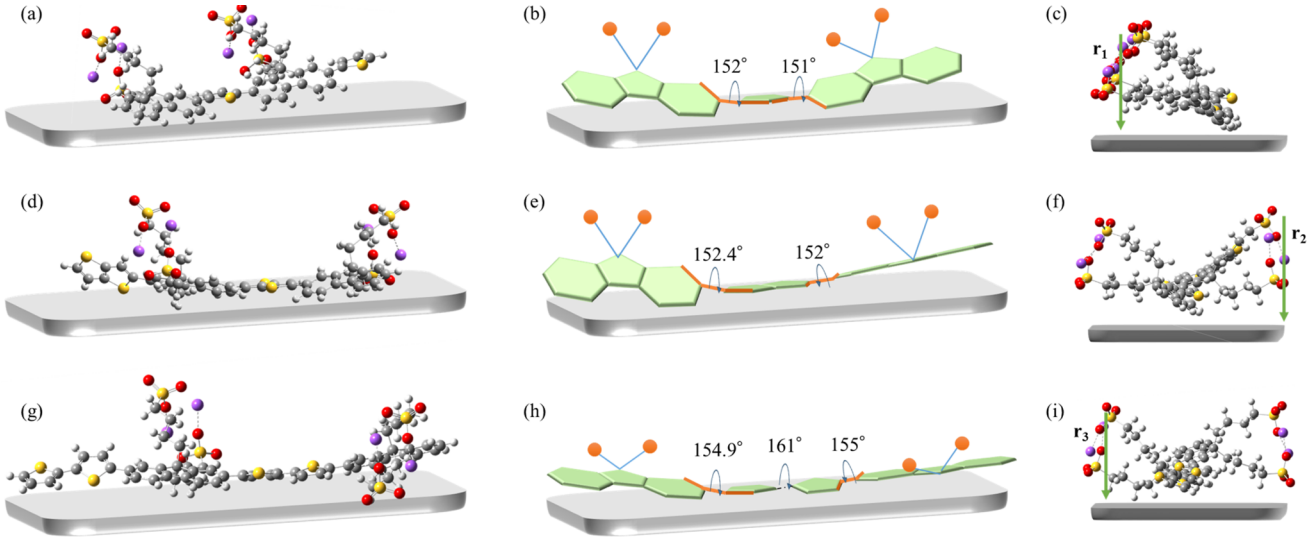


**Figure 3.** Molecular conformation and orientation of CPEs on ITO electrodes. (a) DFT model of PFT-D, (b) schematic of PFT-D arrangement on ITO, (c) side view of PFT-D on ITO, (d) DFT model of PFtT-D, (e) schematic of PFtT-D arrangement on ITO, (f) side view of PFtT-D on ITO, (g) DFT model of PFbT-D, (h) schematic of PFbT-D arrangement on ITO, and (i) side view of PFbT-D on ITO.

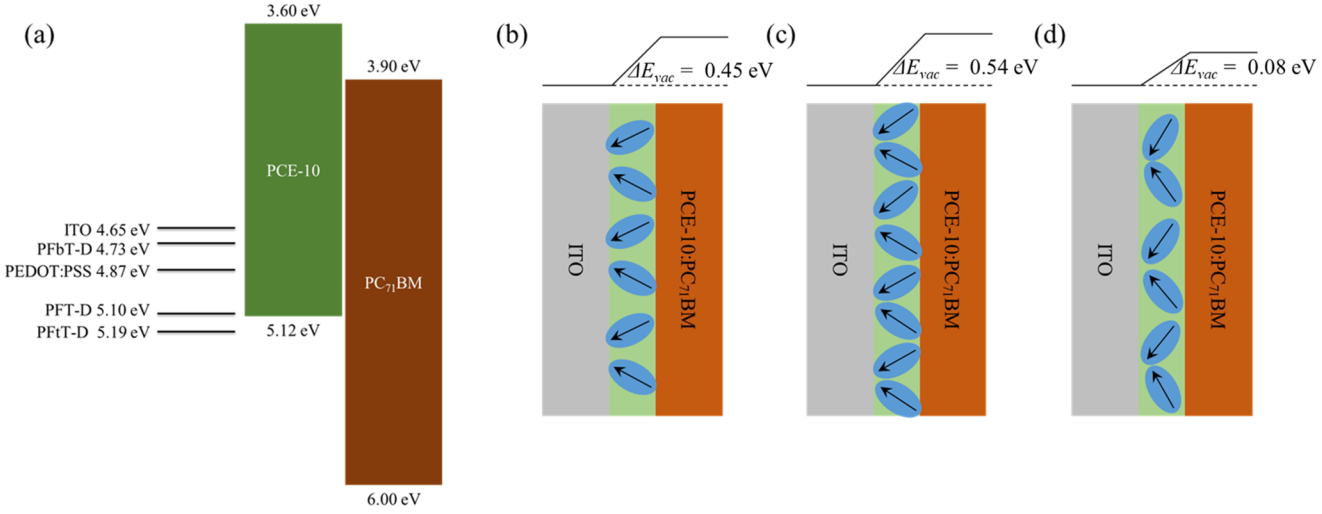


**Figure 4.** (a) Energy-level diagram of OSCs and schematics of the dipole moment orientations of (b) PFT-D, (c) PFtT-D, and (d) PFbT-D.

The WF values of 4.65, 4.87, 5.10, 5.19, and 4.73 eV were obtained for ITO, ITO/PEDOT:PSS, ITO/PFT-D, ITO/PFtT-D, and ITO/PFbT-D, respectively. WFs of the CPE-modified anodes were shifted to lower binding energies. We attribute shifted WFs of the CPE-modified ITO electrodes to the controlled orientation of the molecular dipoles.

From the UPS results, the energy-level diagram for OSCs with CPE HTLs is displayed in Figure 4. The WFs of electrodes with PFT-D and PFtT-D can assure Ohmic contact with the highest occupied molecular orbital (HOMO) level of donor materials and are satisfactorily well matched to facilitate hole extraction. The WFs of ITO coated with CPEs are well matched with the HOMO level of the PCE-10 (HOMO = 5.12), thereby facilitating hole transportation from the photoactive layers to the anodes (Figure 4a). Figure 4b,c shows schematics of the orientations of the dipole moments and shifts in the vacuum levels by the introduction of the CPEs, based on the simulated molecular conformations and orientations shown in Figure 3. When PFT-D and PFtT-D, which have relatively more tilted dihedral angles than PFbT-D, were introduced to the ITO surface, the molecular dipole orientation was more vertical than that with PFbT-D. More vertical molecular dipole orientations correspond to larger dipole moments. As a result, the WF values of the PFT-D- and PFtT-D-covered ITO electrodes were higher than those of ITO/PFbT-D because of the relatively larger vacuum-level shifts.

To study the influence of HTLs on the surface coverage and morphology in OSCs, we utilized AFM. As can be seen in Figure 5, all HTLs provide uniform films with nanoscale features. The root-mean-square roughness ($R_{RMS}$) of PEDOT:PSS was 1.56 nm, indicating a smooth surface for a film of 40 nm thickness. However, the very thin (~5 nm) layers of PFT-D, PFtT-D, and PFbT-D on ITO showed rougher surfaces with nanofiller structures with $R_{RMS}$ > 5 nm, in comparison with the PEDOT:PSS films on ITO. PFtT-D forms a particularly dense nanofiller and uniform film with a relatively low $R_{RMS}$. This suggests that more PFtT-D molecules exist on the ITO surface than other CPE layers contain of their own molecules. The increased number of aligned molecular dipoles


DOI: 10.1021/acsami.7b11164
ACS Appl. Mater. Interfaces 2017, 9, 44060−44069

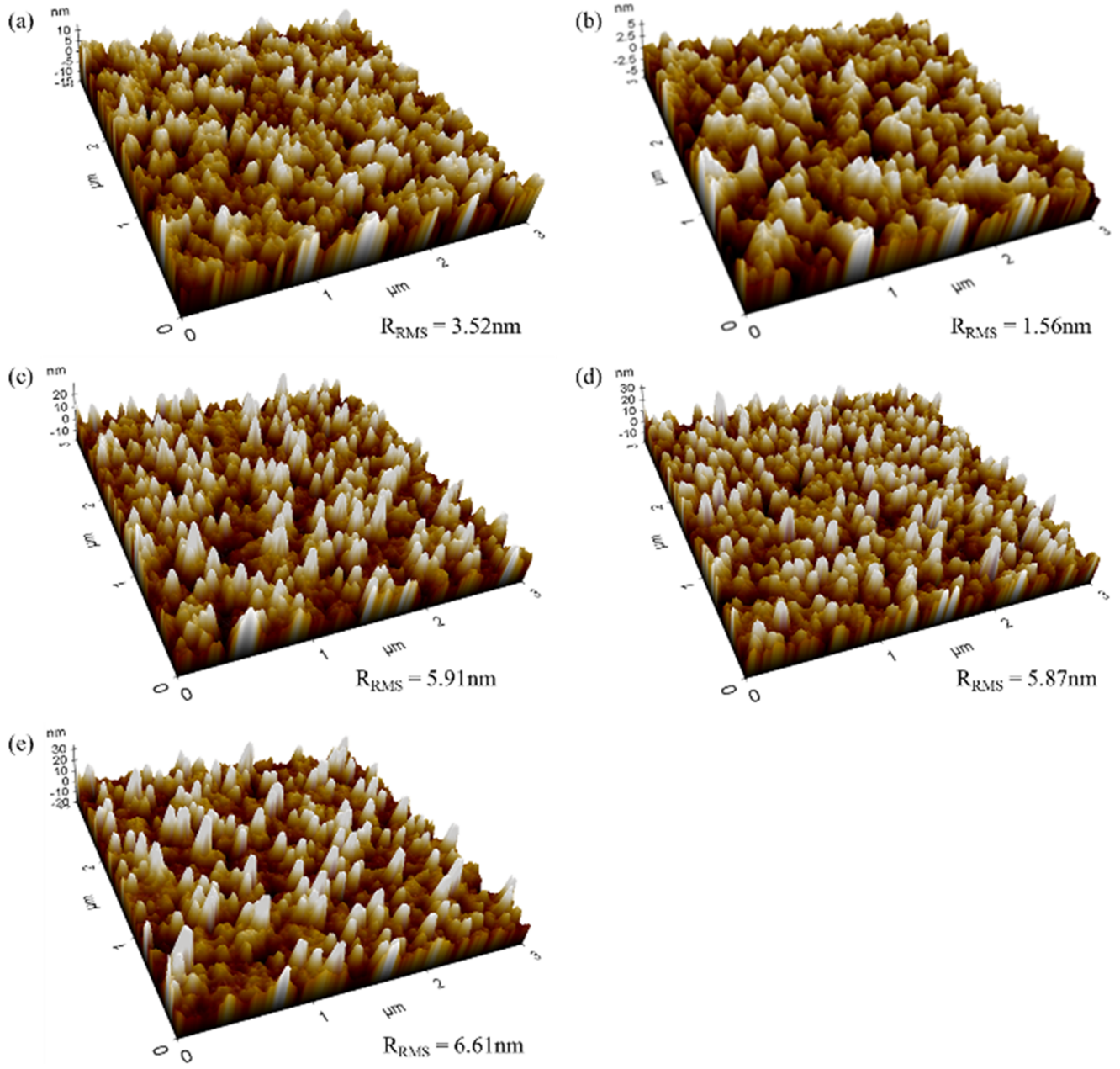


**Figure 5.** Surface topography of (a) ITO, (b) PEDOT:PSS on ITO, (c) PFT-D on ITO, (d) PFtT-D on ITO, and (e) PFbT-D on ITO.

on the surface can increase the electrode dipole moment and WF.[14] By introducing PFtT-D CPE as the HTL on ITO, the molecular dipoles on the surface were increased compared to the PFT-D-covered ITO. As a result, the WF of the ITO/PFtT-D was higher than that of the ITO/PFT-D despite their similar molecular conformations and arrangements. The AFM topographic images of the photoactive layers on PEDOT:PSS and the CPEs are shown in Figure S6 (Supporting Information). These films showed similar uniform surface morphologies, indicating that the molecular orientations of the photoactive layers were not significantly affected by the different HTLs.

However, the photoactive layer−HTL interfaces were further probed because of their decreased $R_{RMS}$ values. The photoactive layer on PFtT-D/ITO exhibits a particularly uniform and smooth surface compared to that on PFT-D and PFbT-D. The AFM images show rough and highly connected interface between PFtT-D and the photoactive layer, which helps to increase the interfacial area. Therefore, higher $J_{sc}$ and FF were achieved with PFtT-D. However, as shown in the AFM images, the CPEs cannot perfectly cover the ITO electrodes. These CPE films with small vacant areas can generate short-circuit paths between the electrodes and organic active layers.[48,49] The paths cause non-Ohmic contact, which is why the CPE HTL-based devices exhibited smaller $V_{oc}$ and FF than the PEDOT:PSS HTL-based devices.

The fabricated OSC devices were stored without encapsulation at 25 °C and 40% humidity under indoor light (~200 lx). The tendencies of efficiency change over approximately 264 h are presented in Figure 6. The devices with CPEs as the HTLs exhibited improved lifetime compared to the reference device because of the neutral nature of CPEs. For the reference device, the PCE rapidly decreased and the half-life of the device was 54 h. However, when PFT-D, PFtT-D, and PFbT-D were introduced as the HTL, the PCE slowly decreased and the


DOI: 10.1021/acsami.7b11164
ACS Appl. Mater. Interfaces 2017, 9, 44060−44069

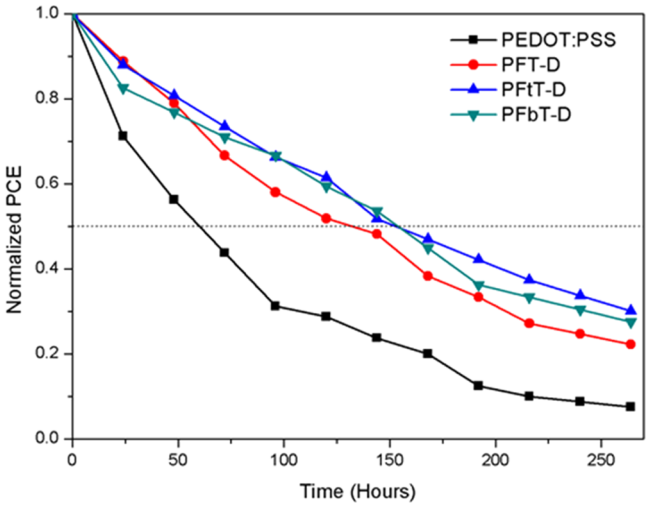


**Figure 6.** Normalized PCE variation as a function of storing time under ambient condition at 25 °C and 40% humidity under ~200 lx interior lighting.

half-lives of the devices became 133, 153, and 154 h, respectively, because of the degradation of $J_{sc}$ and FF. The $J_{sc}$ and FF values decreased as a function of storing time, whereas $V_{oc}$ remained almost constant (Figure S7, see Supporting Information). By introducing CPEs as the OSC HTLs, the half-lives of the devices were more than tripled. We previously reported that changes in HTL surfaces are more important than changes to the blended films of the organic active layers in the degradation of devices with conventional structures.[41] In Figure S8 (Supporting Information), we provide AFM images of the surfaces of HTLs on ITO after 3 days of storage in ambient air. Compared to Figure 5, changes in surface morphology were confirmed in all films via the $R_{RMS}$ values. The surfaces of the CPE films changed less than the PEDOT:PSS film. Surface roughness changes can cause changes in surface potential, which affect the reduction of $J_{sc}$ and FF.[41]

We also fabricated PLEDs by introducing CPEs as the HTL on the ITO electrodes. A super-yellow polymer (Covion) was used as the emitting layer of the PLEDs. The results of luminance and luminance efficiency are shown in Figure 7 and Table 3. The devices with CPEs showed higher performance

**Table 3. Performance of PLEDs**

| HTL | turn-on voltage (V) | maximum luminance (cd/m$^2$) | maximum luminance efficiency (cd/A) |
|---|---|---|---|
| PEDOT:PSS | 3 | 11 518 @ 10 V | 1.10 @ 3 V |
| PFT-D | 3 | 14 628 @ 10 V | 1.71 @ 5 V |
| PFtT-D | 3 | 15 200 @ 10 V | 2.03 @ 4 V |
| PFbT-D | 3 | 12 168 @ 10 V | 0.99 @ 5 V |

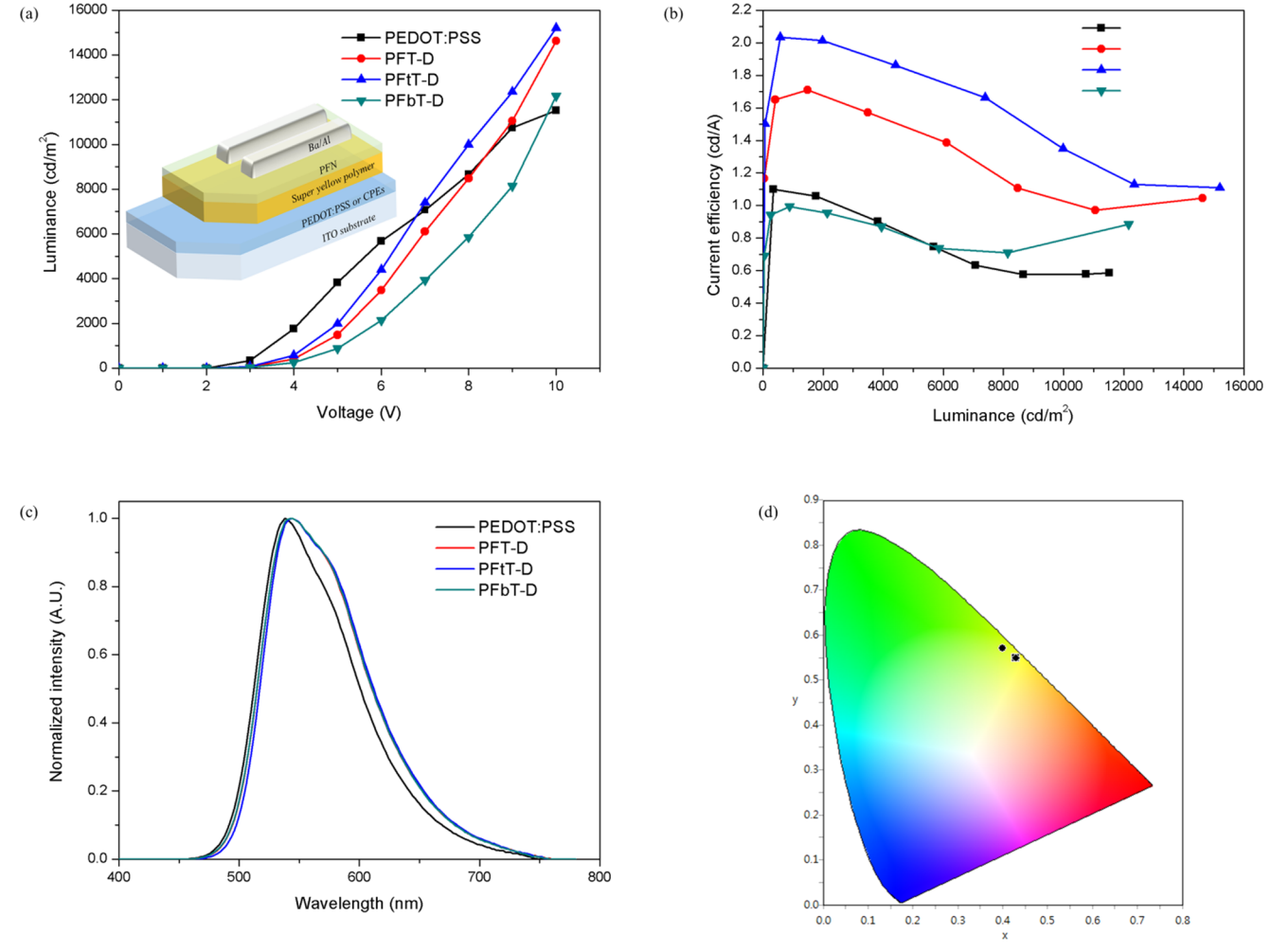


**Figure 7.** (a) Luminance, (b) luminance efficiency, (c) electroluminescence spectra, and (d) image of CIE color coordination of PLEDs.



DOI: 10.1021/acsami.7b11164
ACS Appl. Mater. Interfaces 2017, 9, 44060−44069

than the reference devices. Moreover, the performance tendencies were similar to those of the OSCs because of the effective WFs, which was formed on the surfaces of ITO by the CPE dipole moments. Although the effective WFs of PFT-D and PFtT-D on ITO were lower than those of PEDOT:PSS, the turn-on voltages were equal in all devices. This is because the surface morphologies of the HTL films are similar to those of the OSCs. The HTL's rough surface with nanofiller structure can facilitate the transportation of charge carriers, creating a large contact area at the interface of HTL and organic active layer.[50−52] Thus, the PLED devices with CPE HTLs exhibited enhanced performance relative to the reference devices. At the maximum luminance, the PLED devices with CPEs showed red-shifted electroluminescence spectra and CIE color coordinates of (0.43, 0.55), compared to the PEDOT:PSS-based devices at (0.41, 0.56). It means that the PLED devices with CPE HTLs emitted light, which was closer to pure yellow, because of the reduced interference of the emitted light in the wavelength range over 507 nm.

## CONCLUSIONS

In this study, OSCs and PLEDs were fabricated using three CPEs as the HTLs to understand the effects of the molecular dipole moments formed by the molecular conformations and orientations of CPEs on the electrode surfaces. PFT-D, PFtT-D, and PFbT-D were successfully incorporated into OSCs and PLEDs through solution processing, and the devices showed improved performances and longer-term stability. We used DFT model simulation, UPS analysis, and AFM to understand the relationship between molecular dipole moment and molecular arrangement. In conclusion, PFtT-D, which formed a more vertical orientation in the side chains on the electrode surface and was more uniform and densely nanofiller structured, provided the most effective reduction of the WF of the ITO electrode. This was demonstrated through a general application in OOEDs with the advantages of long-term stability and high performance. These results can contribute to the direction of molecular design for water- or alcohol-soluble CPEs as efficient charge-transporting materials of OOEDs.

## ASSOCIATED CONTENT

### Supporting Information

The Supporting Information is available free of charge on the ACS Publications website at DOI: 10.1021/acsami.7b11164.

Thickness estimation and the optical properties of CPE films, UPS data, morphology images of photoactive layer, and detailed data of long-term stability for OSCs (PDF)

## AUTHOR INFORMATION

### Corresponding Author

*E-mail: dkmoon@konkuk.ac.kr. Tel: +82-2-450-3498. Fax: +82-2-444-0765.

### ORCID

Eui Jin Lee: 0000-0003-4662-361X

### Notes

The authors declare no competing financial interest.

## ACKNOWLEDGMENTS

This research was supported by the Energy Efficiency & Resources Core Technology Program of the Korea Institute of Energy Technology Evaluation and Planning (KETEP), granted financial resource from the Ministry of Trade, Industry & Energy, Republic of Korea (No. 20142020103970), the New & Renewable Energy Core Technology Program of the Korea Institute of Energy Technology Evaluation and Planning (KETEP), and granted financial resource from the Ministry of Trade, Industry & Energy, Republic of Korea (No. 20153010140030).

## REFERENCES

(1) Forrest, S. R.; Thompson, M. E. Introduction: Organic Electronics and Optoelectronics. *Chem. Rev.* **2007**, *107*, 923−925.
(2) Xu, Y.; Zhang, F.; Feng, X. Patterning of Conjugated Polymers for Organic Optoelectronic Devices. *Small* **2011**, *7*, 1338−1360.
(3) Choy, W. C. H.; Chan, W. K.; Yuan, Y. Recent Advances in Transition Metal Complexes and Light-Management Engineering in Organic Optoelectronic Devices. *Adv. Mater.* **2014**, *26*, 5368−5399.
(4) Djurišić, A. B.; Chan, W. K. Organic Optoelectronic Devices. *HKIE Trans.* **2016**, *3733*, 1−40.
(5) Cao, W.; Li, J.; Chen, H.; Xue, J. Transparent Electrodes for Organic Optoelectronic Devices: A Review. *J. Photonics Energy* **2014**, *4*, 040990.
(6) Hsieh, C.-H.; Cheng, Y.-J.; Li, P.-J.; Chen, C.-H.; Dubosc, M.; Liang, R.-M.; Hsu, C.-S. Highly Efficient and Stable Inverted Polymer Solar Cells Integrated with a Cross-Linked Fullerene Material as an Interlayer. *J. Am. Chem. Soc.* **2010**, *132*, 4887−4893.
(7) Chang, Y.-M.; Leu, C.-Y. Conjugated Polyelectrolyte and Zinc Oxide Stacked Structure as an Interlayer in Highly Efficient and Stable Organic Photovoltaic Cells. *J. Mater. Chem. A* **2013**, *1*, 6446−6451.
(8) Wang, F.; Tan, Z.; Li, Y. Solution-Processable Metal Oxides/chelates as Electrode Buffer Layers for Efficient and Stable Polymer Solar Cells. *Energy Environ. Sci.* **2015**, *8*, 1059−1091.
(9) Nian, L.; Gao, K.; Liu, F.; Kan, Y.; Jiang, X.; Liu, L.; Xie, Z.; Peng, X.; Russell, T. P.; Ma, Y. 11% Efficient Ternary Organic Solar Cells with High Composition Tolerance via Integrated Near-IR Sensitization and Interface Engineering. *Adv. Mater.* **2016**, *28*, 8184−8190.
(10) Gaynor, W.; Hofmann, S.; Christoforo, M. G.; Sachse, C.; Mehra, S.; Salleo, A.; McGehee, M. D.; Gather, M. C.; Lüssem, B.; Müller-Meskamp, L.; Peumans, P.; Leo, K. Color in the Corners: ITO-Free White OLEDs with Angular Color Stability. *Adv. Mater.* **2013**, *25*, 4006−4013.
(11) Nakanotani, H.; Higuchi, T.; Furukawa, T.; Masui, K.; Morimoto, K.; Numata, M.; Tanaka, H.; Sagara, Y.; Yasuda, T.; Adachi, C. High-Efficiency Organic Light-Emitting Diodes with Fluorescent Emitters. *Nat. Commun.* **2014**, *5*, No. 4016.
(12) Kang, H.; Kim, G.; Kim, J.; Kwon, S.; Kim, H.; Lee, K. Bulk-Heterojunction Organic Solar Cells: Five Core Technologies for Their Commercialization. *Adv. Mater.* **2016**, *28*, 7821−7861.
(13) Lee, J.-H.; Lee, B. H.; Jeong, S. Y.; Park, S. B.; Kim, G.; Lee, S. H.; Lee, K. Radical Cation-Anion Coupling-Induced Work Function Tunability in Anionic Conjugated Polyelectrolytes. *Adv. Energy Mater.* **2015**, *5*, No. 1501292.
(14) Lee, B. H.; Jung, I. H.; Woo, H. Y.; Shim, H.-K.; Kim, G.; Lee, K. Multi-Charged Conjugated Polyelectrolytes as a Versatile Work Function Modifier for Organic Electronic Devices. *Adv. Funct. Mater.* **2014**, *24*, 1100−1108.
(15) Zilberberg, K.; Meyer, J.; Riedl, T. Solution Processed Metal-Oxides for Organic Electronic Devices. *J. Mater. Chem. C* **2013**, *1*, 4796.
(16) Kim, K.-D.; Lim, D. C.; Hu, J.; Kwon, J.-D.; Jeong, M.-G.; Seo, H. O.; Lee, J. Y.; Jang, K.-Y.; Lim, J.-H.; Lee, K. H.; Jeong, Y.; Kim, Y. D.; Cho, S. Surface Modification of a ZnO Electron-Collecting Layer Using Atomic Layer Deposition to Fabricate High-Performing Inverted Organic Photovoltaics. *ACS Appl. Mater. Interfaces* **2013**, *5*, 8718−8723.
(17) Heo, S. W.; Lee, E. J.; Seong, K. W.; Moon, D. K. Enhanced Stability in Polymer Solar Cells by Controlling the Electrode Work Function via Modification of Indium Tin Oxide. *Sol. Energy Mater. Sol. Cells* **2013**, *115*, 123−128.


DOI: 10.1021/acsami.7b11164
ACS Appl. Mater. Interfaces 2017, 9, 44060−44069

(18) Choi, H.; Park, J. S.; Jeong, E.; Kim, G.-H.; Lee, B. R.; Kim, S. O.; Song, M. H.; Woo, H. Y.; Kim, J. Y. Combination of Titanium Oxide and a Conjugated Polyelectrolyte for High-Performance Inverted-Type Organic Optoelectronic Devices. *Adv. Mater.* **2011**, *23*, 2759−2763.
(19) Tan, Z.; Li, S.; Wang, F.; Qian, D.; Lin, J.; Hou, J.; Li, Y. High Performance Polymer Solar Cells with as-Prepared Zirconium Acetylacetonate Film as Cathode Buffer Layer. *Sci. Rep.* **2014**, *4*, No. 4691.
(20) Yang, L.; Xu, H.; Tian, H.; Yin, S.; Zhang, F. Effect of Cathode Buffer Layer on the Stability of Polymer Bulk Heterojunction Solar Cells. *Sol. Energy Mater. Sol. Cells* **2010**, *94*, 1831−1834.
(21) He, Z.; Zhong, C.; Huang, X.; Wong, W.-Y.; Wu, H.; Chen, L.; Su, S.; Cao, Y. Simultaneous Enhancement of Open-Circuit Voltage, Short-Circuit Current Density, and Fill Factor in Polymer Solar Cells. *Adv. Mater.* **2011**, *23*, 4636−4643.
(22) Song, H. J.; Lee, E. J.; Kim, D. H.; Lee, T. H.; Goh, M.; Lee, S.; Moon, D. K. Solution-Processed Interlayer of Discotic-Based Small Molecules for Organic Photovoltaic Devices: Enhancement of Both the Open-Circuit Voltage and the Fill Factor. *Dyes Pigm.* **2015**, *113*, 210−218.
(23) Song, H. J.; Lee, E. J.; Kim, D. H.; Moon, D. K.; Lee, S. Solution-Processed Interlayer of N-Type Small Molecules for Organic Photovoltaic Devices: Enhancement of the Fill Factor due to Ordered Orientation. *Sol. Energy Mater. Sol. Cells* **2015**, *141*, 232−239.
(24) Qiu, W.; Müller, R.; Voroshazi, E.; Conings, B.; Carleer, R.; Boyen, H.-G.; Turbiez, M.; Froyen, L.; Heremans, P.; Hadipour, A. Nafion-Modified MoOx as Effective Room-Temperature Hole Injection Layer for Stable, High-Performance Inverted Organic Solar Cells. *ACS Appl. Mater. Interfaces* **2015**, *7*, 3581−3589.
(25) Song, H. J.; Shin, G. J.; Choi, K. H.; Lee, S.; Moon, D. K. White Polymer Light Emitting Diode Materials Introducing Dendritic Quinoxaline Derivative: Synthesis, Optical and Electroluminescent Properties. *Synth. Met.* **2014**, *190*, 1−7.
(26) Vosgueritchian, M.; Lipomi, D. J.; Bao, Z. Highly Conductive and Transparent PEDOT:PSS Films with a Fluorosurfactant for Stretchable and Flexible Transparent Electrodes. *Adv. Funct. Mater.* **2012**, *22*, 421−428.
(27) Kim, Y.; Ryu, T. I.; Ok, K. H.; Kwak, M. G.; Park, S.; Park, N. G.; Han, C. J.; Kim, B. S.; Ko, M. J.; Son, H. J.; Kim, J. W. Inverted Layer-By-Layer Fabrication of an Ultraflexible and Transparent Ag Nanowire/Conductive Polymer Composite Electrode for Use in High-Performance Organic Solar Cells. *Adv. Funct. Mater.* **2015**, *25*, 4580−4589.
(28) Jeon, Y.-J.; Lee, S. S.-H.; Kang, R.; Kim, J.-E.; Yeo, J.-S.; Lee, S. S.-H.; Kim, S.-S.; Yun, J.-M.; Kim, D.-Y. Planar Heterojunction Perovskite Solar Cells with Superior Reproducibility. *Sci. Rep.* **2014**, *4*, No. 6953.
(29) Zilberberg, K.; Gharbi, H.; Behrendt, A.; Trost, S.; Riedl, T. Low-Temperature, Solution-Processed MoO $_X$ for Efficient and Stable Organic Solar Cells. *ACS Appl. Mater. Interfaces* **2012**, *4*, 1164−1168.
(30) Steirer, K. X.; Ndione, P. F.; Widjonarko, N. E.; Lloyd, M. T.; Meyer, J.; Ratcliff, E. L.; Kahn, A.; Armstrong, N. R.; Curtis, C. J.; Ginley, D. S.; Berry, J. J.; Olson, D. C. Enhanced Efficiency in Plastic Solar Cells via Energy Matched Solution Processed NiOx Interlayers. *Adv. Energy Mater.* **2011**, *1*, 813−820.
(31) Qiu, M.; Zhu, D.; Bao, X.; Wang, J.; Wang, X.; Yang, R. WO 3 with Surface Oxygen Vacancies as an Anode Buffer Layer for High Performance Polymer Solar Cells. *J. Mater. Chem. A* **2016**, *4*, 894−900.
(32) Zhou, H.; Zhang, Y.; Mai, C.-K.; Collins, S. D.; Nguyen, T.-Q.; Bazan, G. C.; Heeger, A. J. Conductive Conjugated Polyelectrolyte as Hole-Transporting Layer for Organic Bulk Heterojunction Solar Cells. *Adv. Mater.* **2014**, *26*, 780−785.
(33) Lee, B. H.; Lee, J.-H.; Jeong, S. Y.; Park, S. B.; Lee, S. H.; Lee, K. Broad Work-Function Tunability of P-Type Conjugated Polyelectrolytes for Efficient Organic Solar Cells. *Adv. Energy Mater.* **2015**, *5*, No. 1401653.
(34) Choi, M.-H.; Lee, E. J.; Han, J. P.; Moon, D. K. Solution-Processed pH-Neutral Conjugated Polyelectrolytes with One-Atom Variation (O, S, Se) as a Novel Hole-Collecting Layer in Organic Photovoltaics. *Sol. Energy Mater. Sol. Cells* **2016**, *155*, 243−252.
(35) Liu, H.; Huang, L.; Cheng, X.; Hu, A.; Xu, H.; Chen, L.; Chen, Y. N-Type Self-Doping of Fluorinate Conjugated Polyelectrolytes for Polymer Solar Cells: Modulation of Dipole, Morphology, and Conductivity. *ACS Appl. Mater. Interfaces* **2017**, *9*, 1145−1153.
(36) Jung, J. W.; Lee, J. U.; Jo, W. H. High-Efficiency Polymer Solar Cells with Water-Soluble and Self-Doped Conducting Polyaniline Graft Copolymer as Hole Transport Layer. *J. Phys. Chem. C* **2010**, *114*, 633−637.
(37) Xue, Y.; Guo, P.; Yip, H.-L.; Li, Y.; Cao, Y. General Design of Self-Doped Small Molecules as Efficient Hole Extraction Materials for Polymer Solar Cells. *J. Mater. Chem. A* **2017**, *5*, 3780−3785.
(38) Yin, X.; Xie, G.; Peng, Y.; Wang, B.; Chen, T.; Li, S.; Zhang, W.; Wang, L.; Yang, C. Self-Doping Cathode Interfacial Material Simultaneously Enabling High Electron Mobility and Powerful Work Function Tunability for High-Efficiency All-Solution-Processed Polymer Light-Emitting Diodes. *Adv. Funct. Mater.* **2017**, *27*, No. 1700695.
(39) Lee, E. J.; Heo, S. W.; Han, Y. W.; Moon, D. K. An Organic−inorganic Hybrid Interlayer for Improved Electron Extraction in Inverted Polymer Solar Cells. *J. Mater. Chem. C* **2016**, *4*, 2463−2469.
(40) Lee, B. H.; Lee, J.-H.; Jeong, S. Y.; Park, S. B.; Lee, S. H.; Lee, K. Broad Work-Function Tunability of P-Type Conjugated Polyelectrolytes for Efficient Organic Solar Cells. *Adv. Energy Mater.* **2015**, *5*, No. 1401653.
(41) Lee, E. J.; Han, J. P.; Jung, S. E.; Choi, M. H.; Moon, D. K. Improvement in Half-Life of Organic Solar Cells by Using a Blended Hole Extraction Layer Consisting of PEDOT:PSS and Conjugated Polymer Electrolyte. *ACS Appl. Mater. Interfaces* **2016**, *8*, 31791−31798.
(42) Fang, J.; Wallikewitz, B. H.; Gao, F.; Tu, G.; Müller, C.; Pace, G.; Friend, R. H.; Huck, W. T. S. Conjugated Zwitterionic Polyelectrolyte as the Charge Injection Layer for High-Performance Polymer Light-Emitting Diodes. *J. Am. Chem. Soc.* **2011**, *133*, 683−685.
(43) Lee, B. H.; Lee, J.-H.; Jeong, S. Y.; Park, S. B.; Lee, S. H.; Lee, K. Broad Work-Function Tunability of P-Type Conjugated Polyelectrolytes for Efficient Organic Solar Cells. *Adv. Energy Mater.* **2015**, *5*, No. 1401653.
(44) Jo, J. W.; Jung, J. W.; Bae, S.; Ko, M. J.; Kim, H.; Jo, W. H.; Jen, A. K.-Y.; Son, H. J. Development of Self-Doped Conjugated Polyelectrolytes with Controlled Work Functions and Application to Hole Transport Layer Materials for High-Performance Organic Solar Cells. *Adv. Mater. Interfaces* **2016**, *3*, No. 1500703.
(45) Furukawa, Y. Electronic Absorption and Vibrational Spectroscopies of Conjugated Conducting Polymers. *J. Phys. Chem.* **1996**, *100*, 15644−15653.
(46) Liu, F.; Page, Z. A.; Duzhko, V. V.; Russell, T. P.; Emrick, T. Conjugated Polymeric Zwitterions as Efficient Interlayers in Organic Solar Cells. *Adv. Mater.* **2013**, *25*, 6868−6873.
(47) Chen, L.; Xie, C.; Chen, Y. Self-Assembled Conjugated Polyelectrolyte-Ionic Liquid Crystal Complex as an Interlayer for Polymer Solar Cells: Achieving Performance Enhancement via Rapid Liquid Crystal-Induced Dipole Orientation. *Macromolecules* **2014**, *47*, 1623−1632.
(48) Shamjid, P.; Anjusree, S.; Ameen, M. Y.; Reddy, V. S. Performance Enhancement of Polymer Solar Cells by Incorporating Ag Nanoparticles at an Indium Tin oxide/MoO $_3$ Buffer Layer Interface. *Semicond. Sci. Technol.* **2017**, *32*, 065010.
(49) Elumalai, N. K.; Uddin, A. Open Circuit Voltage of Organic Solar Cells: An in-Depth Review. *Energy Environ. Sci.* **2016**, *9*, 391−410.
(50) Lee, E. J.; Heo, S. W.; Han, Y. W.; Moon, D. K. An Organic−inorganic Hybrid Interlayer for Improved Electron Extraction in Inverted Polymer Solar Cells. *J. Mater. Chem. C* **2016**, *4*, 2463−2469.
(51) Earmme, T.; Jenekhe, S. A. High-Performance Multilayered Phosphorescent OLEDs by Solution-Processed Commercial Electron-Transport Materials. *J. Mater. Chem.* **2012**, *22*, 4660−4668.


DOI: 10.1021/acsami.7b11164
*ACS Appl. Mater. Interfaces* 2017, 9, 44060−44069

(52) Yin, Z.; Zheng, Q.; Chen, S.-C.; Cai, D.; Zhou, L.; Zhang, J. Bandgap Tunable Zn 1- X Mg X O Thin Films as Highly Transparent Cathode Buffer Layers for High-Performance Inverted Polymer Solar Cells. *Adv. Energy Mater.* **2014**, *4*, No. 1301404.



DOI: 10.1021/acsami.7b11164
*ACS Appl. Mater. Interfaces* 2017, 9, 44060−44069